Changes in plasma bubble occurrences during geomagnetic storms

Purbi Adhya, Cesar Valladares, The University of Texas at Dallas

Abstract

During geomagnetic storms, prompt-penetration electric fields (PPEF) reach the low-latitude ionosphere and a disturbance dynamo (DD) may follow. PPEF and DD favors and suppresses the development of plasma bubbles respectively through enhancement of the plasma vertical velocities and hence the Pre-Reversal Enhancement (PRE) peak. This poster shows that bubble occurrences, depths, widths and velocities increase during the main phase and decrease during the recovery phase. Plasma density and vertical drift velocity measurements from the C/NOFS satellite and Sym-H index and Bz measurements from the ACE satellite were analyzed to detect bubble occurrences, depths, widths and velocities during the 10 most intense storms throughout the lifetime of the C/NOFS satellite. Statistical analysis shows 1.5 to 1.7 times increase in depths, widths and velocities of the plasma bubbles during the main phase of the storms compared the bubble occurrences during quiet times before and the recovery phase.

Objectives

- Understand the role and effectiveness of PPEF and DD in favoring and/or suppressing plasma bubbles during geomagnetic storms.
- Compare bubble occurrences and characteristics observed during magnetically quiet & disturbed periods.

Bubble detection

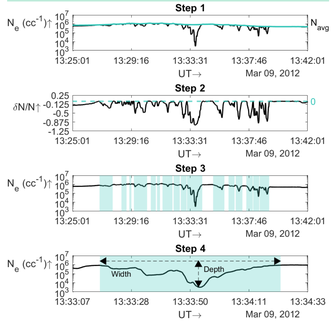

Figure 1: A step-by-step representation of the adopted bubble detection algorithm. The algorithm is described below.

Algorithm:

1. Determine background plasma density (N_{bg}) through averaging raw density measurements (N) and replacing lesser density measurements with the average.
2. Measure difference (δN) between the background density and the raw density and divide by the background density to get the relative change in density (δN/N).
3. Assign bubble boundaries (e.g., t_1 and t_2) at times when the relative change in density turns negative and positive.
4. Calculate depth, width and velocity of each detected bubble using the formulae:
   - $D_{bub} = (\delta N/N)_{max} \times 100$ %
   - $W_{bub} = (t_1 - t_2) \times 7.5$ m
   - $V_{bub} = V_{max}$ m/s

Plasma bubble occurrence patterns during 25-Oct-2011 and 09-Mar-2012 storms

24-Oct-2011 Storm

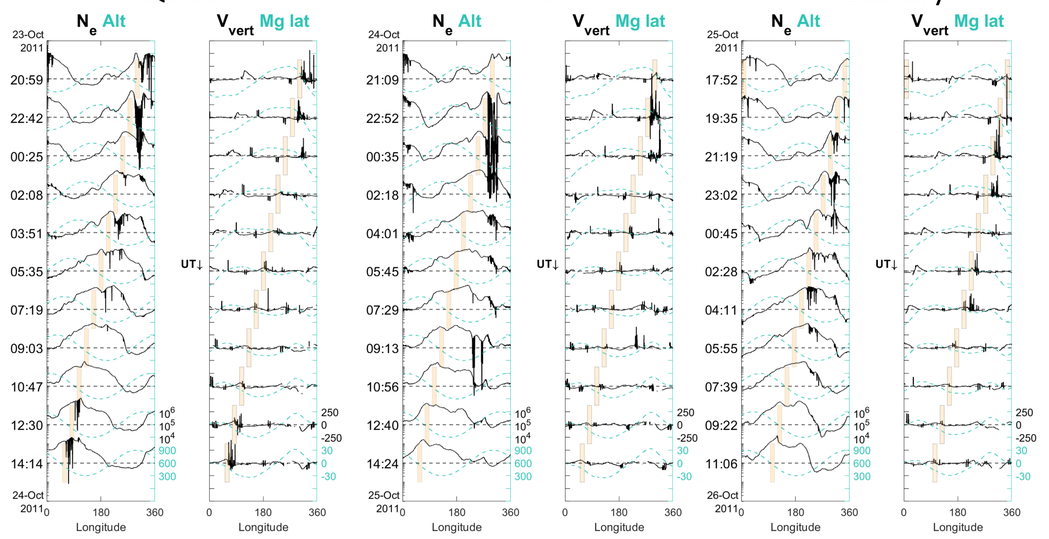

Figure 2: Plasma density, altitude (left panel) and vertical velocity, magnetic latitude (right panel) measurements from the C/NOFS satellite during the quiet time before, and, during the main phase and the recovery phase of the 25-Oct-2011 storm. The yellow patches display the local time hours of 1800 to 1900 when PRE peaks are likely to be observed (Huang, 2018). Satellite orbits were optimum for the observation of plasma bubbles.

09-Mar-2012 Storm

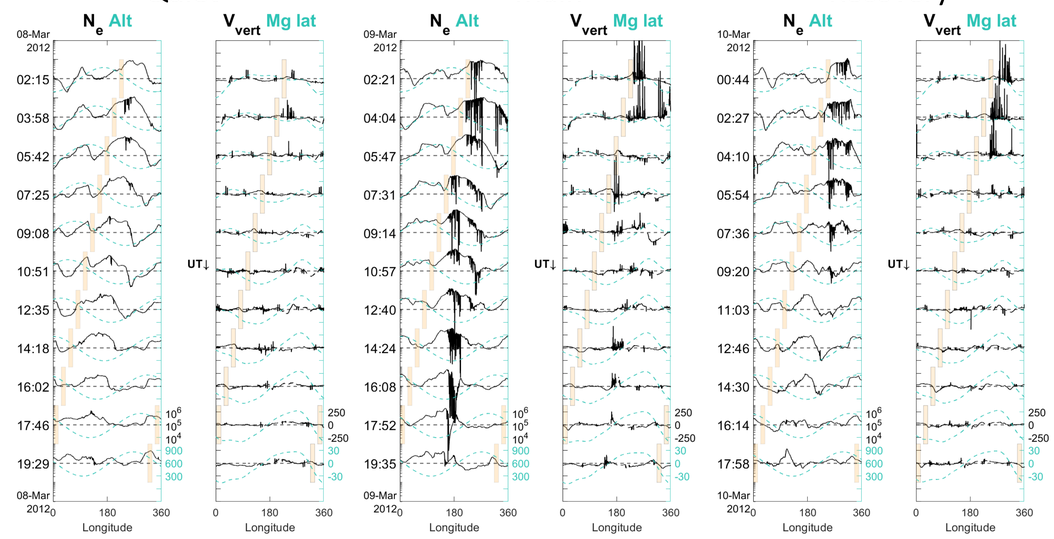

Figure 3: Plasma density, vertical velocity, altitude and magnetic latitude measurements from the C/NOFS satellite during the quiet time before, and, during the main phase and the recovery phase of the 09-Mar-2012 storm. The yellow patches display the local time hours of 1800 to 1900 when PRE peaks are likely to be observed. Satellite orbits were optimum for the observation of plasma bubbles as the magnetic latitudes and the altitudes were low in the post-sunset and post-midnight sector.

Magnetic conditions during 25-Oct-2011 and 09-Mar-2012 storms

24-Oct-2011 Storm

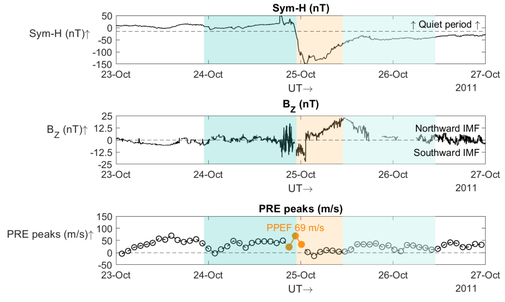

Figure 4: Sym-H index (top panel), Bz component of the IMF (middle panel) and measured PRE peaks (bottom panel) during the 25-Oct-2011 storm. Enhanced PRE peaks caused by PPEF (69m/s) are marked in orange. Quiet, main and recovery phases are shaded with blue, orange and aqua.

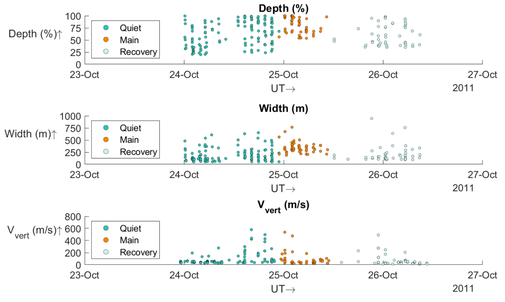

Figure 5: Scatter plot of 75th percentile of bubble depths (top panel), widths (middle panel) and vertical velocities (bottom panel) during the quiet, main and recovery phases of the 25-Oct-2011 storm.

09-Mar-2012 Storm

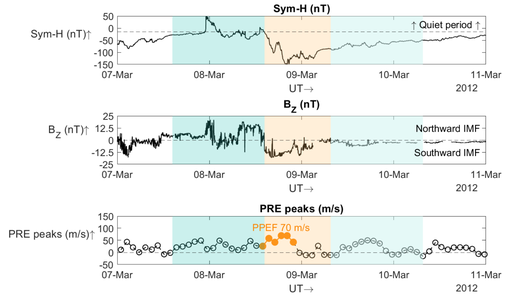

Figure 6: Sym-H index (top panel), Bz component of the IMF (middle panel) and measured PRE peaks (bottom panel) during the 09-Mar-2012 storm. Enhanced PRE peaks caused by PPEF (70m/s) are marked in orange. Quiet, main and recovery phases are shaded with blue, orange and aqua.

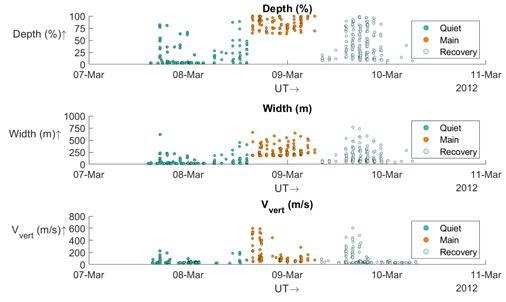

Figure 7: Scatter plot of 75th percentile of bubble depths (top panel), widths (middle panel) and vertical velocities (bottom panel) during the quiet, main and recovery phases of the 09-Mar-2012 storm.

Bubble statistics

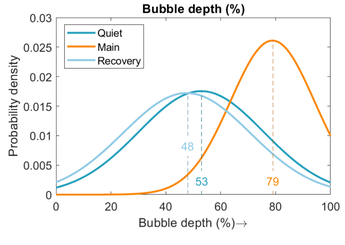

Figure 8: Gaussian fitting of bubble depths (75th percentile for each quiet, main and recovery phase) observed during the 10 most intense storms.

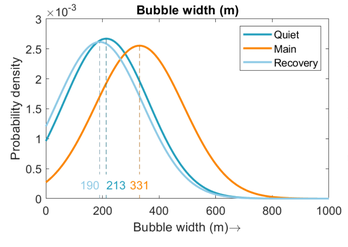

Figure 9: Gaussian fitting of bubble widths (75th percentile for each quiet, main and recovery phase) observed during the 10 most intense storms.

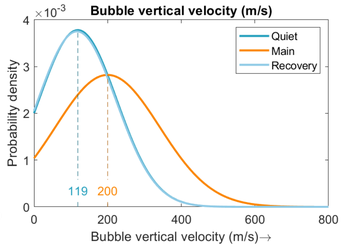

Figure 10: Gaussian fitting of bubble velocities (75th percentile for each quiet, main and recovery phase) observed during the 10 most intense storms.

Conclusions

1. Bubble occurrences are regulated by southward IMF and PPEF during main phase and by disturbance dynamo during recovery phase.
2. Lower bubble production and absence of post-sunset bubbles during the main phase are likely due to the action of the over-shielding effect which takes over the PPEF few hours after the storm commencement. (Abdu, 2011).
3. Bubble occurrences are likely to be controlled by the IMF B_Z and bubble development continues when B_Z remains southwards and stops when B_Z turns northward.
4. Statistical analysis of bubble depths, widths and velocities shows that:
   a. Bubble depths, widths and velocities increase 1.5 to 1.7 times during the main phase.
   b. After the conclusion of the main phase, bubble depths, widths and velocities reduce to the quiet-time magnitude during the recovery phase.